Microstructure, hardening and mechanical properties of hypoeutectic Al-Ce-Ni alloys with Zr and Zr+Sc additions and the effect of ultrasonic melt processing

Suwaree Chankitmunkong[1, a*], Feng Wang[2, b], Chaowalit Limmaneevichitr[3, c], Dmitry G. Eskin[4, 5, d*]

[1]Department of Industrial Engineering, School of Engineering, King Mongkut's Institute of Technology Ladkrabang, Bangkok 10520, Thailand
[2] School of Metallurgy and Materials, University of Birmingham, Birmingham, B15 2SE, United Kingdom
[3]Department of Production Engineering, Faculty of Engineering, King Mongkut's University of Technology Thonburi, 126 Pracha-Utid Rd., Bangmod, Tungkhru, Bangkok, 10140 Thailand
[4]Brunel University London, BCAST, Uxbridge, Middlesex UB8 3PH, United Kingdom
[5]Tomsk State University, Tomsk 634050, Russian Federation

[a*]suwaree.ch@kmitl.ac.th, [b]f.wang.4@bham.ac.uk, [c]chaowalit.lim@mail.kmutt.ac.th, [d]dmitry.eskin@brunel.ac.uk,

Abstract

Ternary Al-Ce-Ni alloys have a potential in the manufacture of automotive and airspace components, as well as in replacing traditional aluminum alloys in high-temperature applications, which is determined by the formation of fine and thermally stable $Al_{11}Ce_3$ and Al_3Ni eutectic. In this study we successfully improved the microstructure and mechanical properties of a hypoeutectic Al4Ce2Ni alloy by using Zr and Zr+Sc additions combined with ultrasonic melt processing and dispersion hardening. As a result, the grain structure of the as-cast alloys was significantly refined and the annealing at 350 °C led to a considerable hardening effect, especially in the alloys with Zr+Sc additions (doubling the hardness). Al_3Zr and $Al_3(Zr,Sc)$ coherent particles were identified as hardening nano-precipitates. The compressive mechanical testing at room and elevated temperatures showed that the additions of Zr and Zr+Sc improved the strength with the additional increase caused by ultrasonic melt processing.

Keywords (3-5 words)

Al-Ce-Ni-Sc-Zr, Aluminum Alloys; Ultrasonic Melt Processing; Nanocomposites; electrical conductivity

1. Introduction

This article has been accepted for publication and undergone full peer review but has not been through the copyediting, typesetting, pagination and proofreading process, which may lead to differences between this version and the Version of Record. Please cite this article as doi: 10.1002/adem.202301045.

Aluminum-cerium alloys represent one of the alternative materials that can find use in automotive application where a combination of light weight, good casting properties, high thermal/electrical conductivity and thermal stability are needed, e.g. in next-generation automotive EV models [1, 2]. Al–Ce based alloys perform well at both room and elevated temperatures owing to the formation of thermally stable intermetallics [1, 3]. Moreover, fine and thermally stable eutectic $Al_{11}Ce_3$ particles produce significant strengthening while preserving ductility [1, 4]. There is a growing trend of using Al–Ce alloys in various applications. Binary Al–Ce alloys have demonstrated good casting properties [3] and ternary Al-4Ce-8Fe [5] and Al-4Ce-2Ni [6] alloys showed potential to be used at elevated temperature with a superior strength and wear resistance as compared to traditional aluminum alloys [1]. When studying different types of ternary eutectic Al-Ce-x alloys, the Al–Ce–Ni system was shown to have a good combination of high mechanical properties at room and elevated temperatures along with very good casting properties [6].

Although the eutectic structure of Al-Ce-Ni alloys is generally rather fine, when the compositions are hypo-eutectic the aluminum dendrites need to be refined to assure defect-free sound castings and improved ductility and toughness [6]. Ultrasonic melt processing (USP) is one of the advanced and environment-friendly techniques to improve the structure of as-cast metallic materials [7, 8], especially those based on Al and Mg [9, 10]. Primary Al_3Zr particles were shown to play important role upon USP providing efficient nucleation sites for the aluminum and eutectic grains [11, 12].

Precipitation (or dispersion) hardening treatment is an efficient way to improve high-temperature mechanical properties through thermally stable nanoprecipitates formed typically by transition elements. Aluminum-scandium (Al-Sc) alloys show excellent mechanical properties at ambient and elevated temperature [13] due to the precipitation of numerous coherent, nanosized Al_3Sc particles with the $L1_2$ crystal structure [14]. At elevated temperature, the Al_3Sc precipitates have high thermal stability because of the low diffusivity of Sc in Al and low coarsening rate [15]. By substituting a portion of scandium (Sc) with zirconium (Zr) in the alloy, it is possible to achieve cost reduction without compromising alloy's desirable mechanical properties at both room temperature and elevated temperatures [16]. The thermal stability and working temperatures of Al-Sc alloys can be increased with addition of Zr (the hardening temperature increasing from 250 to 350-400 °C) [17]. Sc-free Al-Zr alloys also have a potential for dispersion hardening though with a somewhat smaller hardening effect [18]. Recently it was demonstrated that the addition of Sc and Zr to binary Al-1.5Ce alloys resulted in significant hardening through the combination of micron-size $Al_{11}Ce_3$ particles formed upon solidification and nano-sized $Al_3(Sc, Zr)$ precipitates [19]. It was also reported that additions of Zr and Sc refined primary $Al_{11}Ce_3$ particles in hypereutectic Al-Ce alloys through nucleation of $Al_3(Zr, Sc)$ substrates [20].

To the best of our knowledge, there was no previous study on the synergetic effects of USP for the structure refinement combined with dispersion hardening from Al_3Zr ($Al_3(Zr, Sc)$) particles in the Al-Ce-

Ni system. Such a study would have implications for improving the technological, mechanical and functional properties for wider applications in modern manufacturing, e.g. automotive engines and battery enclosures, automotive structural castings, aerospace products, etc.

Thus, this paper is aimed at studying a combination of two mechanisms for the structure and properties control in a promising Al-Ce-Ni-Zr-Sc alloying system: (a) structure refinement by using ultrasonic melt processing and (b) dispersion hardening by precipitates formed during annealing. Alongside a thorough structure examination, we demonstrate an improvement of mechanical properties at room and elevated temperatures while preserving high electric/thermal conductivity.

2. Experimental procedure

2.1 Alloy preparation

The experimental cast alloys of Al-4Ce-2Ni, Al-4Ce-2Ni-0.3Zr and Al-4Ce-2Ni-0.15Zr-0.15Sc (all compositions are in wt%) were prepared from 99.9% pure Al, Al-20% Ce, Al-17% Ni, Al-2% Sc and Al-10% Zr master alloys. The selection of the base composition is based on the previous work by Belov et al. [6]. The solidification range of the experimental alloys was calculated by using Thermo-Calc software (version 2023a) with a Scheil model using the TCAL8 database. This was used in determining the temperature range for ultrasonic processing upon the formation of primary Al_3(Zr, Sc) phase in the alloy. The alloys were melted at 800 °C in a SiC crucible in an electric furnace. The dross and oxide layer were skimmed before the molten metal pouring. The alloy without ultrasonic processing was poured at 730 °C into a thick-walled cylindrical steel mold (90 mm outer diameter, 30 mm inner diameter and 200 mm height), with an approximate solidification rate of 10 °C/s. Ultrasonic melt processing was performed using a Reltec water-cooled magnetostrictive transducer with a driving frequency of 17.5 kHz at 3.5 kW (appr. 25 μm amplitude) equipped with the niobium sonotrode 20 mm in diameter. The sonotrode tip was pre-heated 600 °C and then submerged into the melt. USP was performed in the temperature range from 780 to 730 °C before pouring into the same mold as above. The chemical composition of each alloy is given in Table 1 as an average from three measurements by spark optical emission spectrometry (Foundry Master).

Table 1 Chemical compositions of the experimental alloys

Nominal composition, wt%	Alloy	Experimental composition, wt%				
		Ce	Ni	Zr	Sc	Al

						Balance
Al-4Ce-2Ni	AlCeNi	4.02	2.15	-	-	"
Al-4Ce-2Ni	AlCeNi-USP	4.04	2.17	-	-	"
Al-4Ce-2Ni-0.3Zr	AlCeNiZr	4.01	2.13	0.3		"
Al-4Ce-2Ni-0.3Zr	AlCeNiZr-USP	4.05	2.13	0.3		"
Al-4Ce-2Ni-0.15Zr-0.15Sc	AlCeNiZrSc	4.02	2.16	0.15	0.15	"
Al-4Ce-2Ni-0.15Zr-0.15Sc	AlCeNiZrSc-USP	4.04	2.15	0.15	0.15	"

2.2 Microstructure analysis

Samples for metallographic examination were cut from the center of the castings. The specimens were polished following standard metallographic procedures and the microstructures were observed in an optical microscope (OM, Zeiss Axio Scope.A1). The samples were also anodized in Barker's solution (5% HBF_4 water solution) for about 2 min at 20 VDC and were then examined in the OM under polarized light. The average grain sizes were measured by the linear intercept method according to ASTM E112-10. At least 30 measurements from different 10 images were made on each specimen to the quantitative analysis.

The primary and eutectic phases were characterized by a field emission scanning electron microscope (FE-SEM, Thermo Scientific Apreo S) equipped with an energy-dispersive spectroscopy (EDS) detector. In addition, X-ray diffractometer (XRD, Bruker D8 advance) with a Cu Kα radiation source was used to determine the phase composition of the specimens.

To analyze the nano-precipitates after the aging treatment at 350 °C for 30h, the specimens were cut from the samples containing 0.3% Zr and 0.15% Zr + 0.15% Sc additions and ground to about 100 μm thickness. Then, 3 mm-diameter discs were punched from the foil specimens and further thinned to perforation by precision ion polishing system (Gatan PIPS Model 691). The specimens were examined in a JEOL-2100F transmission electron microscope (TEM). Furthermore, the amount of Zr in the supersaturated Al matrix was measured with EDS in a ZEISS Supra 35 SEM.

2.3 Mechanical and electrical conductivity testing

The specimens 25 mm in radius, 20 mm in thickness were cut from the castings. For dispersion hardening, the specimens were annealed at 350 °C, then quenched in water each 3-h in steps up to 30 h. The annealing temperature was selected following the previous studies [21]. Hardness test was

conducted by using a Brinell Innovatest hardness tester (Nexus 3200) with 625 N load, 2.5 mm ball indenter, and 20 s dwell time. At least ten measurements were made on each specimen.

For compressive testing, the specimens were machined from the central portions of the castings into cylindrical specimens 10 mm long and 5 mm in diameter. The samples were annealed at 350 °C for 30 h prior to testing. Compressive experiments were conducted in a quench-deformation dilatometer DIL 805A/D. The as-cast and annealed (350 °C, 30 h) samples were compressed at 30 °C and 300 °C with a strain rate of 1 s^{-1}. A thermocouple was welded on the specimen to monitor the temperatures during testing. The specimen was initially fixed in the chamber between punches and then the force was applied from the initial length of 10 mm to 5 mm at 30 °C. For the high-temperature condition, the sample was set up in the chamber and then heated up to 300 °C with a heating rate of 10 °C/s, held for 3 minutes, and subsequently compressed from the initial length of 10 mm to 5 mm at the same strain rate. Finally, it was quenched with argon gas flow. Compressive true stress–true strain curves were automatically recorded during the entire test cycle.

The electrical conductivity was measured on the surface specimens that were annealed at 350 °C for 30 h by using a Sigmatest 2.069 (Forester Instruments) at a frequency of 120 kHz.

3. Results and Discussion

3.1 Thermo-Calc calculations for the solidification sequence

We intended to use the mechanism of structure refinement through USP that involved enhanced heterogenous nucleation and fragmentation of primary Al_3Zr particles due to ultrasonic cavitation. In order to select the proper temperature range that will facilitate this mechanism, we calculated the sequence of phase formation in the Al-4Ce-2Ni alloy with Zr and Zr+Sc additions, Fig. 1. The results showed that the addition of 0.3 wt% Zr to the base alloy resulted in the increase of liquidus temperature, with the formation of the Al_3Zr primary phase at 755 °C, Fig. 1a. When the amount of Zr decreased to 0.15 wt% and 0.15 wt% Sc was added, the primary Al_3(Zr, Sc) phase started to form at 700 °C, Fig. 1b. Then the eutectic phases were formed in the range 645 to 630 °C. Therefore, the USP in the experiment was applied in the temperature range of 780 – 690 °C, i.e. in the temperature range from the fully liquid state into the primary Al_3Zr (Al_3(Zr,Sc)) phase formation range. According to our previous work, such a temperature range will result in the best results in terms of the primary phase refinement [22]. Note that the USP done at lower temperatures, e.g. during the eutectic solidification, would typically result in the coarsening of the eutectic due to the acoustic energy introduced, which would slow down the eutectic solidification [7].

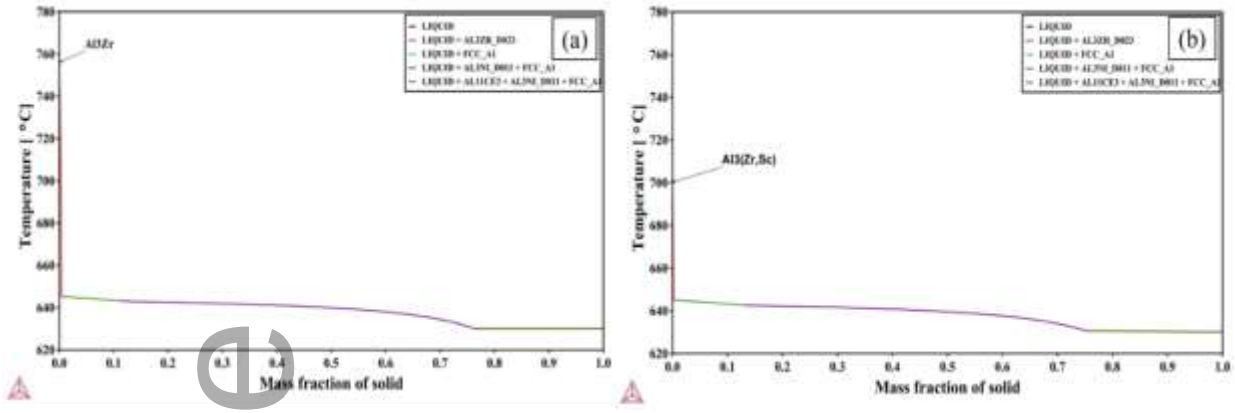

Fig. 1 Scheil simulation for solidification of an Al-4Ce-2Ni alloy with: (a) the addition of 0.3% Zr, and (b) the addition of 0.15% Sc and 0.15% Zr.

3.2 Microstructure and phase analysis

The as-cast microstructures of the ternary AlCeNi alloy and the alloys with additions AlCeNiZr and AlCeNiZrSc alloys without USP are shown in Error! Reference source not found. **a-c** and with USP in Error! Reference source not found. **d-f**, respectively.

One can see that the structure consisted of Al dendrites and relatively large eutectic patches. The additions of Zr or Zr+Sc did not change much the grain structure in the alloys without USP. With the USP, the structure became more uniform, irrespective of the Zr (Sc) additions, while the dendrites were refined after USP with Zr and Zr+Sc additions as can be seen more clearly in **Fig. 4**. One can notice primary Al_3Zr particles in **Fig. 2b** and **2e**. The difference is that primary particles agglomerated in the alloys without USP while after USP they were fragmented and dispersed. The alloys with Zr and Sc did not show any large primary particles, most likely due to the much lower amount Zr.

The eutectic constituents in the alloys were confirmed to comprise $Al_{11}Ce_3$ (Al_4Ce) and Al_3Ni phases in accordance with Thermocalc calculations (Fig.1). **Figure 3** shows XRD spectra with the $Al_{11}Ce_3$ and Al_3Ni phases agreeing with the Thermocalc result in Fig. 1.

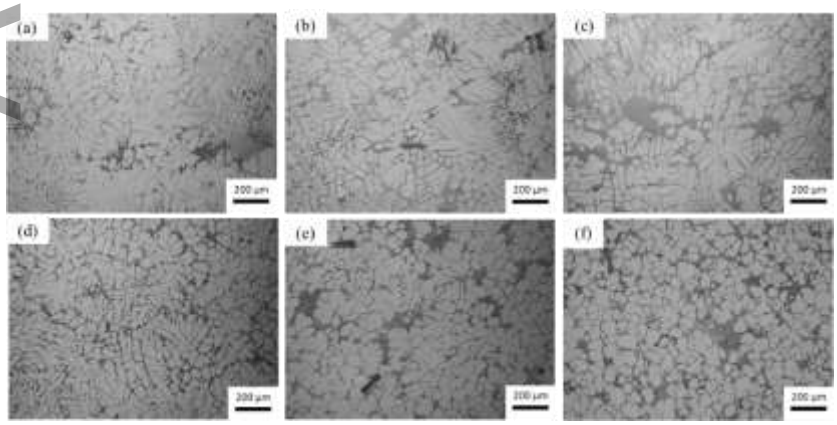

Fig. 2 Optical macrographs of as-cast specimens, showing grain and eutectic structure, without USP: (a) AlCeNi, (b) AlCeNiZr, (c) AlCeNiZrSc, and with USP: (d) AlCeNi-USP, (e) AlCeNiZr-USP, (f) AlCeNiZrSc-USP.

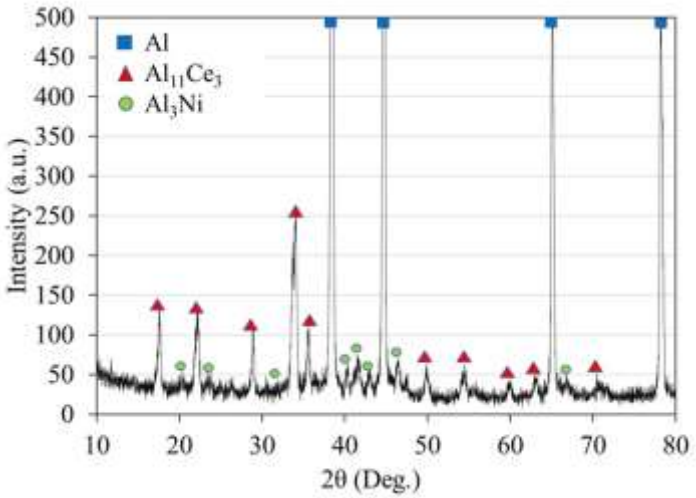

Fig. 3 XRD patterns of the as-cast AlCeNi alloy.

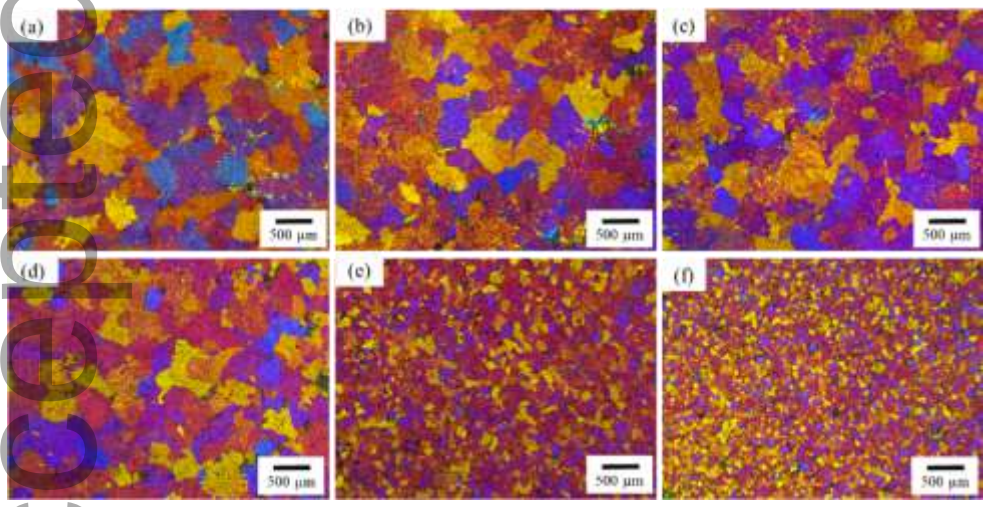

Fig. 4 Optical polarized micrographs of the as-cast specimens, demonstrating grain structures: without USP: (a) AlCeNi, (b) AlCeNiZr, (c) AlCeNiZrSc, and with USP: (d) AlCeNi-USP, (e) AlCeNiZr-USP, (f) AlCeNiZrSc-USP.

Figure 4 shows the grain structure in the tested alloys (optical micrographs in polarized light). These results confirmed that the addition of Zr or Zr+Sc to the base alloy did not change much the grain structure (**Fig. 2a-c** and **Fig. 4a-c**), while the situation dramatically changed upon USP when the grain structure became significantly refined (**Fig. 5e**), especially upon joint Zr and Sc additions **(Fig. 4f)**. These observations were further supported by the quantitative data in Fig. 5, with the

average grain size decreasing from about 350 μm in the base alloy to approximately 120 and 85 μm in the alloys with Zr and Zr+Sc additions subjected to USP. These results confirmed that the mechanisms of structure refinement induced by the presence of Zr and USP were successfully employed in the structure control of the tested Al-Ce-Ni alloys.

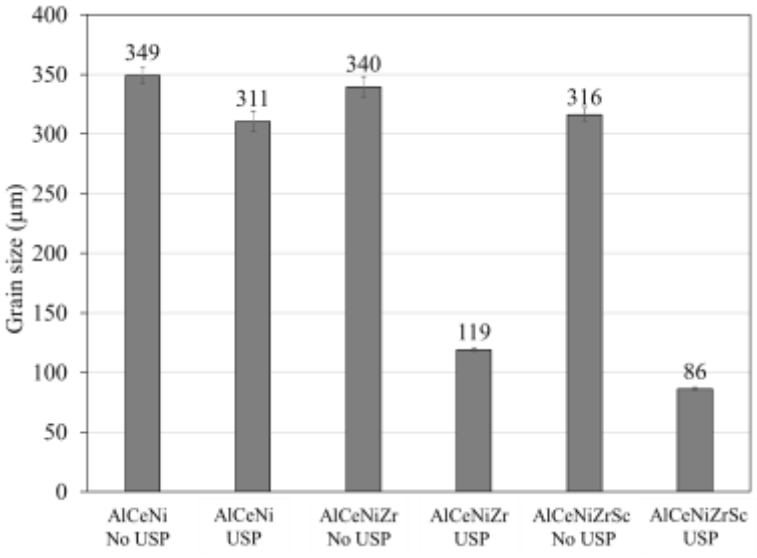

Fig. 5 Grain size of the alloys with and without USP

These mechanisms have been studied in detail elsewhere for other groups of Al alloys and include the heterogeneous nucleation of primary Al_3Zr particles on the oxide inclusions activated by ultrasonic cavitation followed by the refinement through fragmentation of these particles by shock-waves and acoustic flows induced by cavitation [7, 11, 12, 23].

Figures 6 and **7** demonstrate the results of these mechanisms. One can see that the USP resulted in a significant refinement of primary Al_3Zr in the alloy with 0.3% Zr (compare **Fig. 6a** and **b**), while in the alloy with 0.15% Zr and 0.15% Sc no primary phase was found without USP but USP triggered the nucleation of this phase and then refined it (compare **Fig. 6c** and **d**). It is well known that Zr and Sc tend to supersaturate aluminum solid solution upon solidification rather than form primary particles, which explains the absence of these particles in the alloy containing lesser amount of Zr and solidified without USP. Ultrasonic cavitation facilitates nucleation of primary phases on activated inclusions and therefore triggers the formation of the primary particles while also fragmenting them. **Figure 7** presents the EDS mapping of some particles, confirming that they contain Zr, Sc. There was also some dissolved Ce (not shown here). The location of the particles inside the grains (**Fig. 6 b**, **d**, **Fig. 7a**) gives a clue to their role as nucleation substrates. It is interesting that Sc tend to form an outer layer on the Al_3Zr particles (**Fig. 7i**), which is similar to that already reported by us earlier [24]. This Sc-rich layer may improve the nucleating ability of the Al_3Zr phase by changing the surface structure, making it close to Al_3Sc. The role of Ce in Al_3Zr needs to be studied in more detail.

Therefore, the mechanisms of USP-induced structure refinement in aluminum alloys with Zr were demonstrated to work in the Al-Ce-Ni alloying system as well.

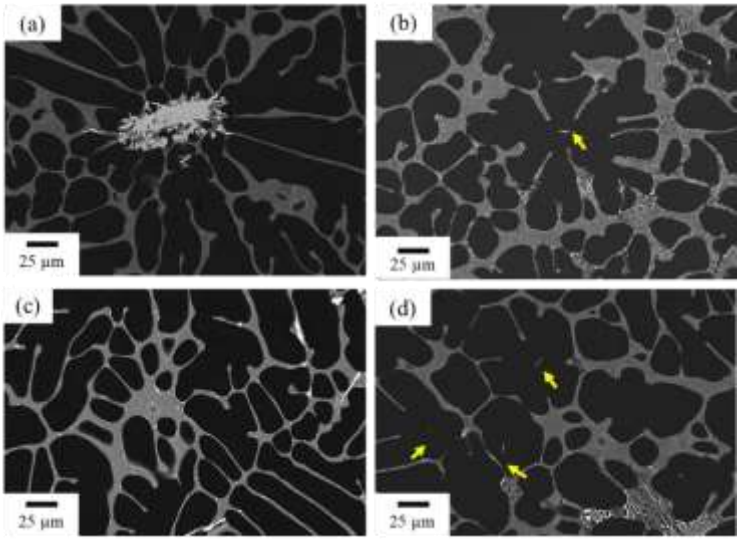

Fig. 6 SEM images of primary Al_3Zr particles: (a) AlCeNiZr, (b) AlCeNiZr-USP, (c) AlCeNiZrSc and (d) AlCeNiZrSc-USP. Yellow arrows shown the refined primary Al_3Zr particles.

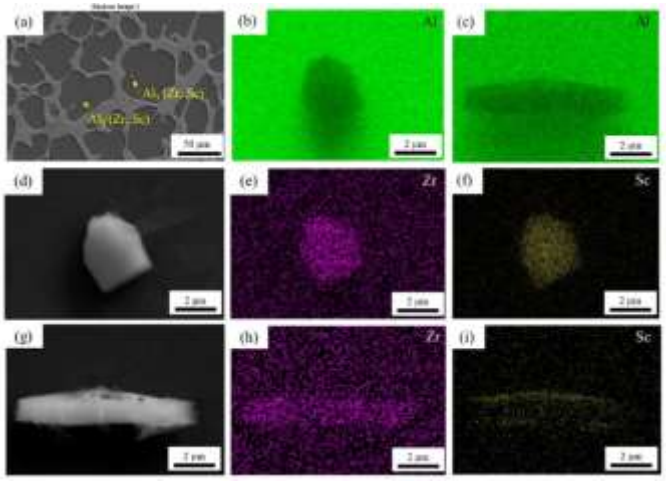

Fig. 7 SEM images of primary particles (a, d, g) in the AlCeNiZrSc-USP alloy; and corresponding EDS mapping (b, c) Al, (e, h) Zr, (f, i) Sc.

3.3 Dispersion hardening and electrical conductivity

Figure 8 shows the hardness of the as-cast alloys (a) as well as the hardening upon annealing at 350 °C (b). The hardness of the as-cast alloys did not change much with addition of Zr, Sc or USP, with a slight tendency to increase in the alloys with Zr/Sc additions and decrease with USP in these alloys. The base alloy did not show any hardening effect upon annealing, while the alloys with 0.3% Zr demonstrated a moderate hardening effect (appr. 15 HB) and the alloys with 0.5% Zr and 0.15% Sc

had a significant hardening effect (appr. 40 HB, or doubling the initial hardness). As one can see from **Fig. 8b**, USP had a rather small effect on hardening, most noticeable in the alloys with 0.3% Zr. Note that the substantial grain refinement (**Fig. 4**) was not reflected on the hardness or hardening effect.

The electrical conductivity measurements in **Fig. 9** demonstrated that additions of Zr and Zr+Sc resulted in overall decrease of the conductivity that was somewhat restored upon annealing, especially in the alloys containing Zr+Sc. USP did not have any significant effect of this property. It is well known that the electrical (and thermal) conductivity depends on the amount of alloying elements in the supersaturated solid solution, stresses induced by coherent precipitates and the overall presence of interfaces. Zr and Zr+Sc tend to supersaturate the aluminum solid solution upon solidification. Therefore, we see a substantial decrease in the conductivity of the as-cast alloys with the additions of Zr and Zr+Sc. Although USP triggered nucleation of the primary Al_3Zr phase (which in principle should lead to the lesser amount of Zr available for supersaturation), we did not see any consequence of that for the conductivity. Therefore, we can assume that the amount of Zr in the solid solution was close to its limit of supersaturation at the given cooling rate. **Figure 10** gives the measurements of the Zr concentration retained in the solid solution after casting. It can be seen that the average concentration of retained Zr is between 0.15 and 0.18%, with USP only slightly affecting this, mostly through the formation of primary particles (larger particles formed with USP deplete the solid solution of Zr). Therefore, the amount of Zr in the solid solution will be similar in the alloys with 0.3 and 0.15% Zr, which explains the similar values of conductivity. Sc in the solid solution had apparently a smaller effect on the conductivity. After precipitation of Al_3Zr or Al_3(Zr, Sc) phases, the conductivity was restored. But it remained smaller in the AlCeNiZr alloys than in the AlCeNiZrSc alloys, which might be a consequence of the chosen annealing temperature. This temperature, i.e. 350 °C, was sufficiently high for the complete precipitation of Al_3(Zr,Sc) phase while might be too low of the complete precipitation of Al_3Zr [25]. Although both these phases have a similar $L1_2$ structure and are coherent with the matrix as demonstrated in **Figs. 11** and **12**, the kinetics of their precipitation is different [13] with the Al_3(Zr, Sc) phase precipitating at a higher pace and having a core-shell structure (enriched Sc core and Zr-rich shell) that is more efficient in hardening and slowing down the coarsening [26, 27].

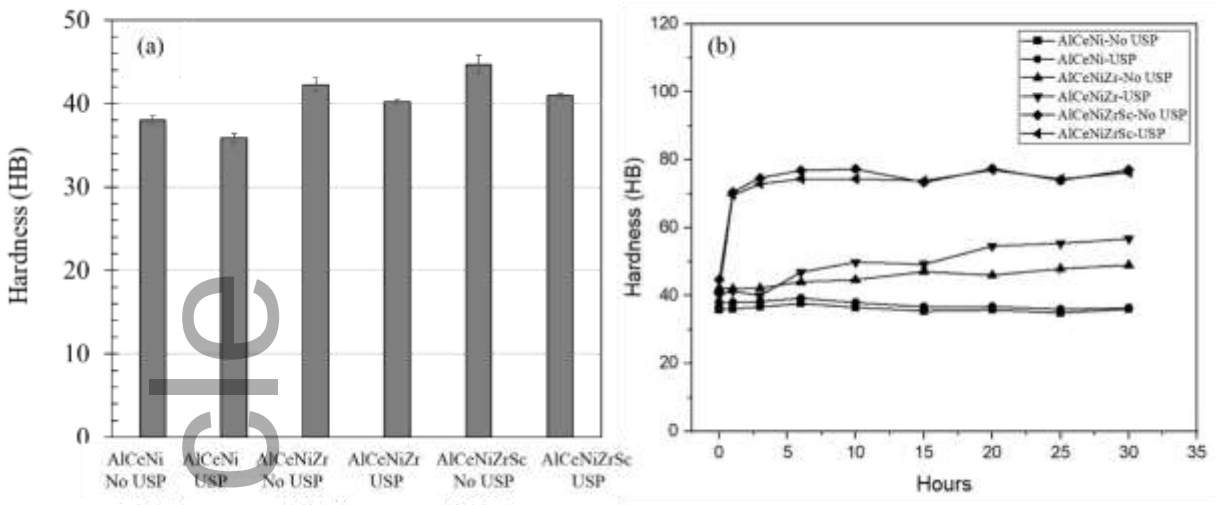

Fig. 8 The hardness of (a) as-cast alloys and (b) the alloys annealed at 350 °C for up to 30 h.

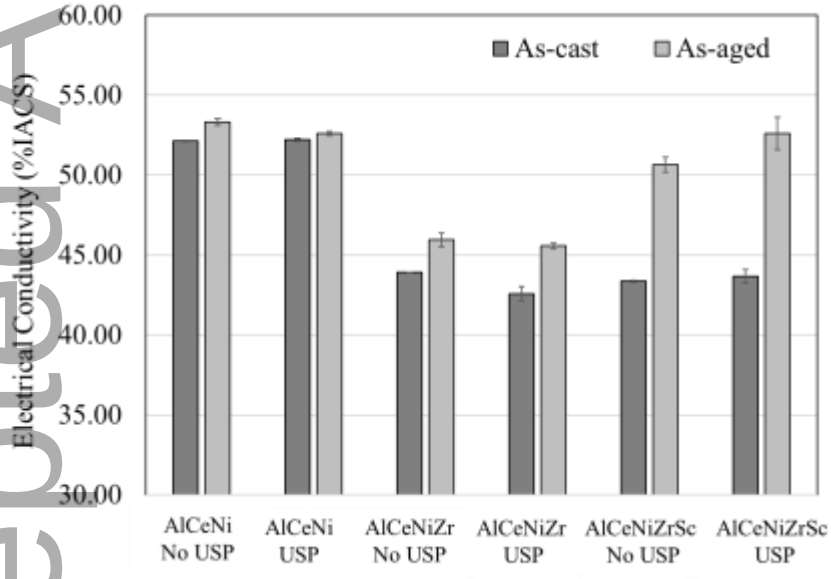

Fig. 9 Electrical conductivity of the as-cast and annealed (350 °C, 30 h) alloys.

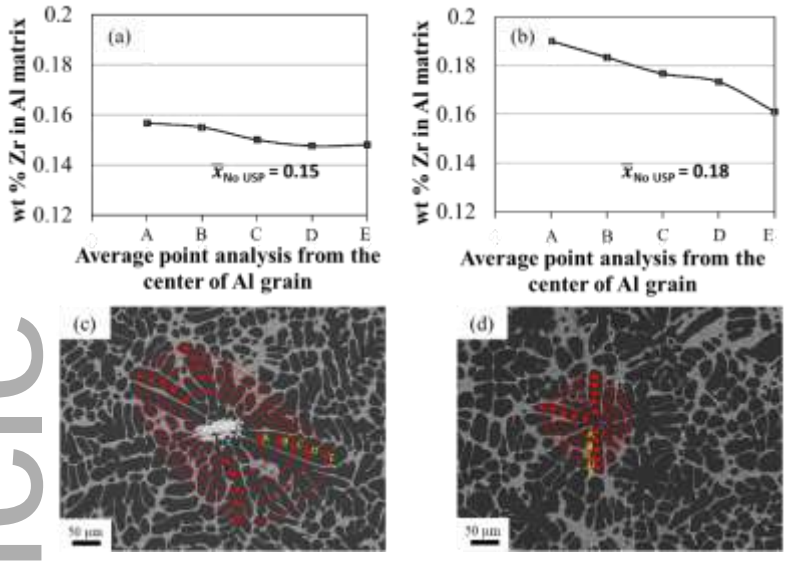

Fig. 10 Measurements of Zr retained in the aluminum solid solution after solidification: (a, c) AlCeNiZr and (b, d) AlCeNiZr-USP. Error bars are smaller than the data point symbols.

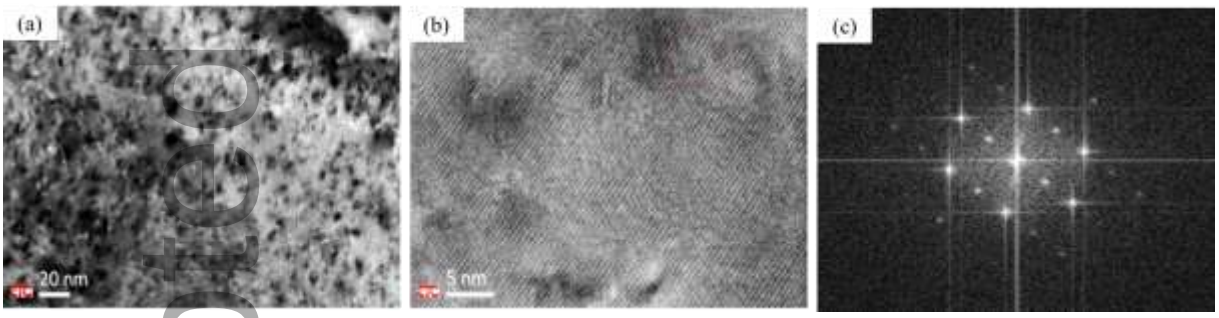

Fig. 11 TEM images showing the Al_3Zr precipitates in the annealed (350 °C, 30 h) AlCeNiZr alloy: (a) morphology of Al_3Zr precipitates distributed in Al matrix; (b) HRTEM image of the Al_3Zr precipitates, and (c) the FFT related to (b) confirming the presence of $L1_2$ type nanoprecipitates in this region.

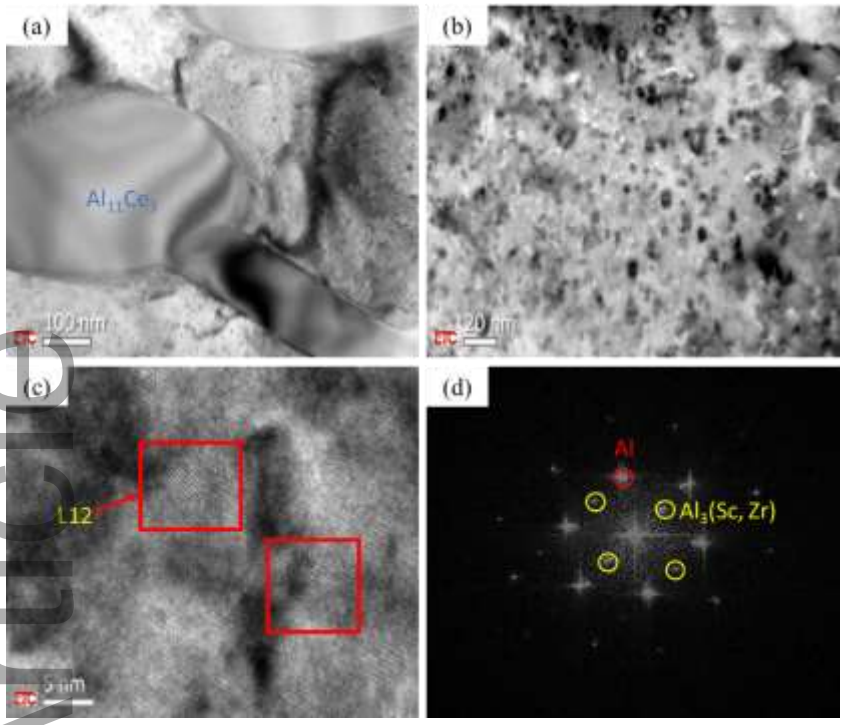

Fig. 12 TEM images of annealed (350 °C, 30 h) AlCeNiZrSc alloy: (a) the distribution of precipitates in the eutectic region, (b) a higher magnification of Al_3(Zr, Sc) precipitates, (c) HRTEM image showing $L1_2$ nanoprecipitates, and (d) the FFT related to (c) confirming the presence of $L1_2$ type nanoprecipitates in the marked area in (c).

3.4 Mechanical properties at room and elevated temperatures

Al-Ce-Ni alloys have a potential to be used in automotive and airspace applications as castings and, possibly, forgings. To assess the deformation behavior of these alloys at room and elevated temperatures, they were tested upon compression after being annealed at 350 °C for 30 h. The results are shown in **Figs. 13** and **14**.

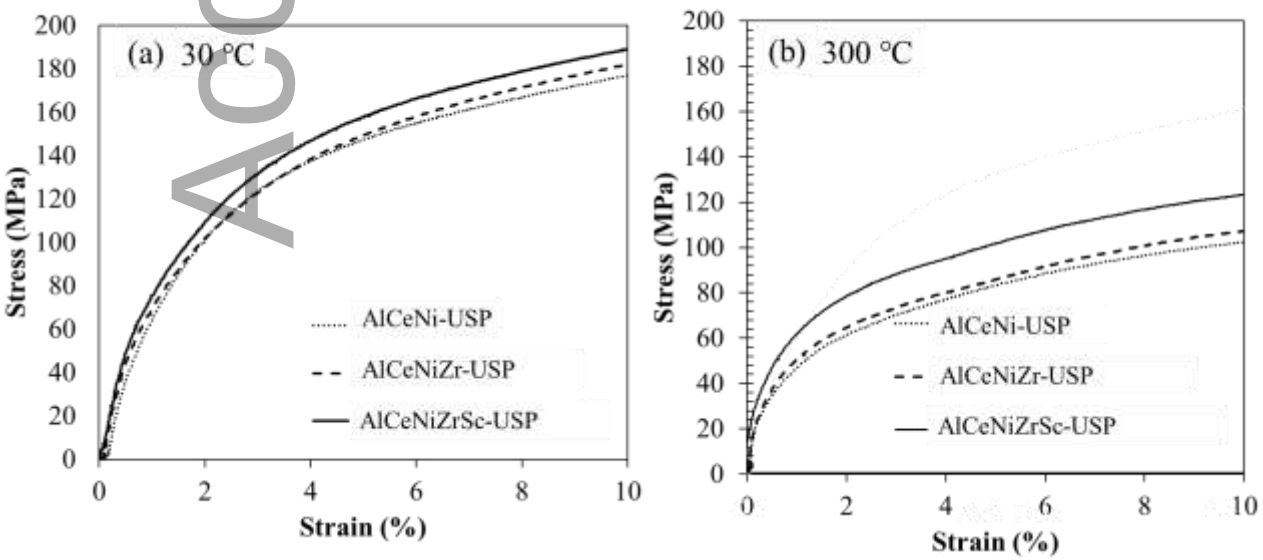

Fig. 13 Compressive stress–strain curves of the dispersion hardened alloys subjected to USP at two deformation temperatures (a) 30 °C and (b) 300 °C.

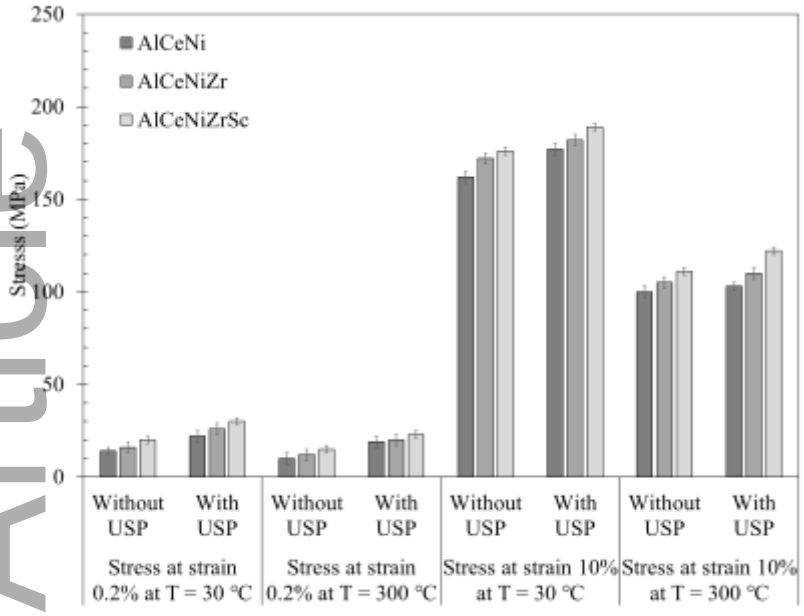

Figure 14 The 0.2% proof yield strength and the stress at 10% strain of the dispersion hardened alloys tested at 30 and 300°C.

One can see that the additions of Zr and Zr+Sc consistently improved the yield stress and overall strength of the base alloy, e.g. the Zr+Sc addition increased the room temperature yield stress from 14 to 20 MPa and from 10 to 15 at 300 °C; and the compressive stress at 10% strain increased from 162 to 176 MPa at RT and from 100 to 111 MPa at 300 °C. USP gave an additional contribution to the compressive strength, reaching a yield stress of 30 MPa and a 10%-stress of 189 MPa for the AlCeNiZrSc-USP alloy at room temperature. Similar improvements were for the samples tested at 300 °C.

The main reasons for the improvement of the compressive strength properties with Zr and Zr+Sc were the dispersion hardening induced by the Al_3Zr and $Al_3(Zr, Sc)$ precipitates as was demonstrated in Section 3.3. As the annealing was done at the temperatures above the testing temperature, the hardening precipitates should remain relatively stable and the hardening effect should be preserved. Additional contribution form USP came from the grain refinement (see **Figs. 4** and **5**). This grain refinement resulted in a more uniform distribution of intermetallics and ensured better deformability of the alloys with Zr and Zr+Sc, adding to the compressive strength.

4. Conclusions

The grain structure of hypoeutectic Al4Ce3Ni alloys can be significantly refined by using the combination of Zr or Zr+Sc additions and ultrasonic melt processing in the temperature range of the primary Al_3Zr intermetallic formation. The mechanisms known from the earlier studies involve the enhanced heterogeneous nucleation of Al_3Zr on nonmetallic inclusions with subsequent refinement of the primary particles by fragmentation induced by ultrasonic cavitation. These refined particles are then act as substrates for aluminum grains. Zr and Sc that supersaturate the aluminum solid solution upon solidification enable dispersion hardening upon annealing at 350 °C with either Al_3Zr or Al_3(Zr, Sc) precipitates, the latter offering a significantly better hardening response. There is a clear link between the hardening response and the concentration of Zr retained in the solid solution after solidification. The synergetic effect of both the structure refinement upon solidification and the dispersion hardening upon annealing leads to the improved mechanical properties at room and elevated (300 °C) temperatures.

Acknowledgements

The authors gratefully acknowledge FE-SEM Centre, School of Engineering, King Mongkut's Institute of Technology Ladkrabang and the financial support under project number RE-KRIS/FF66/29. D.E. acknowledges the financial support from EPSRC (UK) under project grant PAAM (EP/W00593X/1). S.C. gratefully acknowledges BCAST (UK) for TEM facility support.

Declaration of competing interest

The authors declare that they have no known competing financial interests or personal relationships that could have appeared to influence the work reported in this paper.

References

[1] Z.C. Sims, O.R. Rios, D. Weiss, P.E. Turchi, A. Perron, J.R. Lee, T.T. Li, J.A. Hammons, M. Bagge-Hansen, T.M. Willey, High performance aluminum–cerium alloys for high-temperature applications, Materials Horizons 4(6) (2017) 1070-1078.

[2] F. Czerwinski, Cerium in aluminum alloys, Journal of Materials Science 55(1) (2020) 24-72.

[3] Z.C. Sims, D. Weiss, S.K. McCall, M.A. McGuire, R.T. Ott, T. Geer, O. Rios, P.A.E. Turchi, Cerium-based, intermetallic-strengthened aluminum casting alloy: high-volume co-product development, JOM 68(7) (2016) 1940-1947.

[4] D. Weiss, Improved high-temperature aluminum alloys containing cerium, J. Mater. Eng. Perform. 28(4) (2019) 1903-1908.

[5] Y.-H. Mashal, M. Kassem, A. Waheed, Stability, wear, and corrosion characteristics of rapidly solidified high temperature Al-8Fe-4Ce alloy, Tribology and Interface Engineering Series, Elsevier2005, pp. 703-708.
[6] N.A. Belov, E.A. Naumova, D.G. Eskin, Casting alloys of the Al–Ce–Ni system: microstructural approach to alloy design, Materials Science and Engineering: A 271(1) (1999) 134-142.
[7] G.I. Eskin, D.G. Eskin, Ultrasonic Treatment of Light Alloy Melts, CRC Press 2015.
[8] S. Chankitmunkong, D.G. Eskin, C. Limmaneevichitr, Structure refinement, mechanical properties and feasibility of deformation of hypereutectic Al–Fe–Zr and Al–Ni–Zr alloys subjected to ultrasonic melt processing, Materials Science and Engineering: A 788 (2020) 139567.
[9] A.P. Khrustalyov, A.A. Kozulin, I.A. Zhukov, M.G. Khmeleva, A.B. Vorozhtsov, D. Eskin, S. Chankitmunkong, V.V. Platov, S.V. Vasilyev, Influence of titanium diboride particle size on structure and mechanical properties of an Al-Mg alloy, Metals 9(10) (2019) 1030.
[10] H. Kotadia, M. Qian, A. Das, Microstructural modification of recycled aluminium alloys by high-intensity ultrasonication: Observations from custom Al–2Si–2Mg–1.2 Fe–(0.5, 1.0) Mn alloys, Journal of Alloys and Compounds 823 (2020) 153833.
[11] T.V. Atamanenko, D.G. Eskin, L. Zhang, L. Katgerman, Criteria of grain refinement induced by ultrasonic melt treatment of aluminum alloys containing Zr and Ti, Metallurgical and Materials Transactions A 41(8) (2010) 2056-2066.
[12] D. Eskin, Ultrasonic processing of aluminium alloys above the liquidus: the role of Zr, MATEC Web of Conferences, EDP Sciences, 2020, p. 06002.
[13] L. Toropova, D. Eskin, M. Kharakterova, T. Dobatkina, Advanced Aluminum Alloys Containing Scandium: Structure and Properties, Gordon an Breach OPA 1998.
[14] E.A. Marquis, D.N. Seidman, Nanoscale structural evolution of Al_3Sc precipitates in Al(Sc) alloys, Acta Mater. 49(11) (2001) 1909-1919.
[15] S.-I. Fujikawa, Impurity diffusion of scandium in aluminium, Defect and Diffusion Forum, Trans Tech Publ, 1997, pp. 115-120.
[16] A. De Luca, D.C. Dunand, D.N. Seidman, Scandium-enriched nanoprecipitates in aluminum providing enhanced coarsening and creep resistance, Light Metals 2018, Ed. O. Martin, Springer, Cham, 2018, pp. 1589-1594.
[17] C.B. Fuller, D.N. Seidman, D.C. Dunand, Mechanical properties of Al(Sc,Zr) alloys at ambient and elevated temperatures, Acta Materialia 51(16) (2003) 4803-4814.
[18] M. Song, Y. He, S. Fang, Effects of Zr content on the yield strength of an Al-Sc alloy, Journal of Materials Engineering and Performance 20 (2011) 377-381.
[19] C.N. Ekaputra, J.U. Rakhmonov, D. Weiss, J.-E. Mogonye, D.C. Dunand, Microstructure and mechanical properties of cast Al-Ce-Sc-Zr-(Er) alloys strengthened by $Al_{11}Ce_3$ micro-platelets and $L1_2$ Al_3(Sc,Zr,Er) nano-precipitates, Acta Materialia 240 (2022) 118354.
[20] J. Ye, K. Dai, Z. Wang, J. Chen, M. Gao, R. Guan, Beneficial effects of Sc/Zr addition on hypereutectic Al–Ce alloys: Modification of primary phases and precipitation hardening, Materials Science and Engineering: A 835 (2022) 142611.
[21] C.B. Fuller, D.N. Seidman, Temporal evolution of the nanostructure of Al(Sc,Zr) alloys: Part II-coarsening of $Al_3(Sc_{1-x}Zr_x)$ precipitates, Acta Materialia 53(20) (2005) 5415-5428.
[22] W. Feng, D. Eskin, T. Connolley, J.-W. Mi, Influence of ultrasonic treatment on formation of primary Al_3Zr in Al–0.4 Zr alloy, Transactions of Nonferrous Metals Society of China 27(5) (2017) 977-985.
[23] A. Priyadarshi, M. Khavari, T. Subroto, M. Conte, P. Prentice, K. Pericleous, D. Eskin, J. Durodola, I. Tzanakis, On the governing fragmentation mechanism of primary intermetallics by induced cavitation, Ultrasonics Sonochemistry 70 (2021) 105260.
[24] N.A. Belov, D.G. Eskin, A.A. Aksenov, Multicomponent Phase Diagrams: Applications for Commercial Aluminum Alloys, Elsevier 2005.
[25] N. Belov, A. Alabin, D. Eskin, V. Istomin-Kastrovskii, Optimization of hardening of Al–Zr–Sc cast alloys, Journal of Materials Science 41 (2006) 5890-5899.
[26] C.B. Fuller, J.L. Murray, D.N. Seidman, Temporal evolution of the nanostructure of Al(Sc,Zr) alloys: Part I – Chemical compositions of $Al_3(Sc_{1-x}Zr_x)$ precipitates, Acta Materialia 53(20) (2005) 5401-5413.
[27] E. Clouet, L. Laé, T. Épicier, W. Lefebvre, M. Nastar, A. Deschamps, Complex precipitation pathways in multicomponent alloys, Nature Materials 5(6) (2006) 482-488.

Additions of Zr or Zr+Sc combined with ultrasonic melt processing significantly improve the microstructure and mechanical properties of a hypoeutectic Al4Ce2Ni alloy. The grain structure of the as-cast alloys is significantly refined and the annealing at 350 °C leads to a considerable hardening effect, doubling the hardness in the alloys with Zr+Sc additions. The compressive mechanical properties are improved at room temperature and 300 °C.